




Enhanced energy storage properties on calcium modified strontium barium niobate lead-free ferroelectric relaxor ceramics

Shaobo Guo^{1,2,3,*} , Zhen Liu¹, Chunhua Yao¹, Fei Cao¹, and Genshui Wang^{1,2,3,*}

¹Key Laboratory of Inorganic Functional Materials and Devices, Shanghai Institute of Ceramics, Chinese Academy of Sciences, 1295 Dingxi Road, Shanghai 200050, People's Republic of China

²Center of Materials Science and Optoelectronics Engineering, University of Chinese Academy of Sciences, Beijing 100049, People's Republic of China

³State Key Laboratory of High Performance Ceramics and Superfine Microstructure, Shanghai Institute of Ceramics, Chinese Academy of Sciences, 1295 Dingxi Road, Shanghai 200050, People's Republic of China

Received: 16 December 2022

Accepted: 21 May 2023

Published online:

2 June 2023

© The Author(s), under exclusive licence to Springer Science+Business Media, LLC, part of Springer Nature 2023

ABSTRACT

In this study, calcium modified strontium barium niobate ($\text{Ca}_x\text{Sr}_{0.75-x}\text{Ba}_{0.25}\text{Nb}_2\text{O}_6$, CSBN- x , $0 \leq x \leq 0.20$) lead-free ferroelectric relaxor ceramics were prepared by conventional solid-state reaction technique and their crystal structure, morphology, dielectric, ferroelectric and energy storage properties were studied comprehensively. The modified CSBN ceramics present pure tetragonal tungsten bronze structure (TTBS) in the whole studied composition range. The introduction of calcium elevates the ferroelectric to paraelectric transition temperature remarkably while has little influence on the relaxor behavior of strontium barium niobate system. Although the maximum polarization (P_{\max}) and remnant polarization (P_r) of CSBN- x increase with x , the difference of the two values ($P_{\max}-P_r$) is also heightened, thus improving its energy storage performance. The optimal energy storage properties, *i.e.* high recoverable energy storage density W_{rec} (1.21 J/cm^3) and energy storage efficiency η (87.7%), ultrahigh temperature stability (the fluctuations on W_{rec} and η are within 2% and 3% over the range of 25 °C–120 °C, respectively) are achieved in $\text{Ca}_{0.05}\text{Sr}_{0.70}\text{Ba}_{0.25}\text{Nb}_2\text{O}_6$ composition. These excellent performance properties qualify this environment-friendly SBN-based ferroelectric relaxor ceramics as a promising alternative in energy storage application.

Address correspondence to E-mail: guoshaobo@mail.sic.ac.cn

1 Introduction

Due to their high-power density, fast charge–discharge speed and good temperature stability, dielectric capacitors are considered to be promising for energy storage application, including electric vehicles, mobile electronics, pulsed power devices and [1, 2]. Generally, linear dielectrics (LDs), ferroelectrics (FEs), anti-ferroelectrics (AFEs) and relaxor ferroelectrics (RFEs) are considered as four kinds of promising dielectrics in these fields [3, 4]. The recoverable energy density (W_{rec}) and energy storage efficiency (η) are key parameters of a dielectric capacitor to evaluate its energy storage performance, entirely depending on the saturation polarization (P_{max}), remnant polarization (P_r), and breakdown strength (BDS) of the materials [5, 6]. Relaxor ferroelectrics with polar nanoregions (PNRs) usually demonstrate diffuse phase transition and slim hysteresis loops, which result in low P_r and high P_{max} , thus expecting superior energy storage densities and energy conversion efficiencies [6–8]. Moreover, due to the diffusion phase transition nature, the permittivity of RFEs is usually insensitive to temperature change within a certain range, which favors the improvements of temperature stability in energy storage application [9]. Over the past decades, huge research progress for dielectric energy storage capacitors has been made in perovskite structure RFEs including BaTiO₃-based, NaNbO₃-based, Bi_{0.5}Na_{0.5}TiO₃-based and K_{0.5}Na_{0.5}NbO₃-based ceramics [8, 9, 10, 11, 12, 13].

Tetragonal tungsten bronze structure (TTBS) ferroelectrics are the second largest group of ferroelectrics after perovskite structure, which features connection of BO₆ octahedrons by sharing common vertex and forming three types of interstices (A1, A2 and C sites) accessible for different cations. According to cations occupancy situation, this kind of materials can be categorized into three groups: fully filled (A and C sites all occupied), filled (all A sites occupied and C sites empty) and unfilled (partial A sites occupied and C sites empty) [14]. Many investigations have been performed among filled TTBS ceramics for energy storage owing to their superior dielectric properties [15]. For unfilled TTBS compounds, the special structure of A-site vacancies and multi-interstices becomes the origin of relaxation and provides great freedom for composition design and performance improvement, [16] suggesting the

potential as candidates for energy storage capacitors. Thus, the innovative design of unfilled TTBS energy storage ceramics may help to understand the underlying mechanism among structure, composition and performance, and provide an effective material for high performance energy storage application.

As a typical unfilled TTBS compound, Sr_xBa_{1-x}Nb₂O₆ (SBN, $x = 0.25 - 0.75$) solid solution has been widely studied for its excellent electro-optic, pyroelectric and photorefractive properties [17–20]. The crystallographic non-equivalent sites of SBN structure and its compositional flexibility provide various possibilities of physical properties modification [21, 22]. For example, changing the Sr/Ba ratio could have a strong impact on the phase transition and properties due to the preferential occupation of A-site ions. When increasing Sr/Ba ratio, SBN materials experience a change from normal ferroelectrics to relaxor ferroelectrics. The higher Sr/Ba ratio is, the greater the phase transformation diffusion is. Meanwhile in the high Sr compositions, the ferroelectric-paraelectric phase transformation temperature decreases while the dielectric maximum at this point increases [18, 20]. All facts above suggest that SBN with high Sr composition, as typical relaxor ferroelectrics, should be favorable for energy storage application. Bai et al. [23] synthesized (Sr_{0.5}Ba_{0.5})_{1+x}Nb_{2-x}Fe_xO₆ ceramics that acquired a W_{rec} of 0.680 J/cm³ and an η of 83.6% at $x = 0.04$. Tang et al. [24] obtained a W_{rec} of 0.19 J/cm³ and an η of 86.37% in Sr_{0.60}Ba_{0.40}Nb₂O₆ ceramics under 60 kV/cm electric field. Rao et al. [25] reported that Sr_{0.70}Ba_{0.30}Nb_{2-x}O_{6-x} wt% MgO ceramics exhibit a $W_{rec} = 0.93$ J/cm³ and an $\eta = 89.4\%$ at 157 kV/cm when $x = 0.5$. In general, due to the slim characteristics of the hysteresis loops of the SBN ceramics with high Sr compositions, the energy storage efficiency η is high. However, in consequence of suffering from low polarization in these compositions, the recoverable energy density W_{rec} is quite poor.

Several methods, including doping and utilizing various synthesis techniques, [23, 25, 26] have been introduced to modify electric properties of SBN. Among them, Ca-substitution is considered as an effective way to enhance the dielectric, pyroelectric and ferroelectric properties of SBN, since (Ca,Ba)Nb₂O₆ (CBN) crystal exhibits higher spontaneous polarization (~ 35 μ C/cm²) than SBN crystal (~ 27 μ C/cm²) [27]. Our previous results showed that Ca-substitution at the A sites of unfilled SBN can

improve the ferroelectric and pyroelectric performance in $\text{Ca}_{0.15}(\text{Sr}_{0.5}\text{Ba}_{0.5})_{0.85}\text{Nb}_2\text{O}_6$ ceramics [28]. Further studies in $\text{Ca}_x\text{Sr}_{0.3-x}\text{Ba}_{0.7}\text{Nb}_2\text{O}_6$ system also revealed that the saturated polarization increased monotonically with increasing Ca content, indicating that the ferroelectricity in unfilled SBN can be greatly enhanced by Ca addition [29]. It is also reported that Ca-substitution can be capable of improving the ferroelectric properties of filled SBN systems, such as $\text{Sr}_{2-x}\text{Ca}_x\text{NaNb}_5\text{O}_{15}$ (SCNN) and $(\text{Sr}_{0.6}\text{Ba}_{0.4})_4\text{Na}_2\text{Nb}_{10}\text{O}_{30}$ (SBNN) [30, 31].

In this article, we introduced Ca into the typical TTBS $\text{Sr}_{0.75}\text{Ba}_{0.25}\text{Nb}_2\text{O}_6$ lead-free ferroelectric relaxor ceramics in order to improve the energy storage performance. Effect of Ca content on the structure and electric properties of $\text{Ca}_x\text{Sr}_{0.75-x}\text{Ba}_{0.25}\text{Nb}_2\text{O}_6$ ($x = 0, 0.05, 0.10, 0.15, 0.20$ abbreviated as CSBN-0, CSBN-5, CSBN-10, CSBN-15, CSBN-20) ceramics was systematically investigated. Enhanced energy storage performance is achieved in Ca-substituted SBN matrix with high Sr composition, indicating this environmentally friendly ferroelectric relaxor ceramic as a promising alternative in energy storage application.

2 Experimental procedures

The CSBN- x ceramics are synthesized by conventional solid-state reaction method using Nb_2O_5 (99.3%), BaCO_3 (99%), SrCO_3 (99%), and CaCO_3 (99%) as raw materials and weighted stoichiometrically. The starting materials are mixed in polyurethane jars and ball milled via ethanol for 24 h using agate balls with a rotation speed of 115 rpm. The mass ratio of the starting materials to milling ball is 1: 1.5. The starting materials are mixed and ball milled for 24 h via ethanol. The mixed powder is calcined at 1260 °C for 2 h and then re-milled and pressed into circular pellets with a diameter of 13 mm. The pellets are air sintered at 1360 °C for 4 h. The sintered pellets are polished to 0.15 mm thickness and coated with silver paste in order to take the electric properties measurement.

The crystal structure of the samples is confirmed by X-ray diffraction (XRD, D/MAX-2550 V; Rigaku, Tokyo, Japan) technique using Cu K α radiation. The microstructure of the ceramics is observed by the TM3000 Tabletop Microscope (Hitachi, Tokyo, Japan) on the fresh surface of samples. The porosity

percentage of the samples were tested and calculated via Archimedes method. Measurements of the dependence of dielectric constant and loss on temperature are performed in the range 20 °C–200 °C using a Hewlett Packard LCR meter (Model HP4284A; Agilent Technologies Japan Ltd., Hyogo, Japan) at different frequencies from 100 Hz to 1 MHz. Polarization hysteresis loops are characterized by applying an electric field of sinusoidal waveform at a frequency of 10 Hz using commercial ferroelectric analyzer (TF Analyzer 2000, aixACCT, Aachen, Germany) assisted with high-voltage power supply (Trek Inc, Medina, NY).

3 Results and discussion

3.1 Phase structure and microstructure

Figure 1a displays the XRD pattern of CSBN- x ceramics. The diffraction peaks, being indexed according to JCPDF39-0265, present a pure tetragonal tungsten bronze structure. No obvious splits of diffraction peaks can be detected in all samples. The enlarged patterns for the (410) diffraction peak (around 29°–30°) of all samples shown in the Fig. 1b are found to shift towards higher 2θ angles, indicating the shrinkage of lattice with the increase of the Ca content. The detailed structure properties are further analyzed via Rietveld refinement method using FullProf software. The R-pattern R_p , R-weighted pattern R_{wp} and Goodness-of-fit χ^2 are used as the numerical criteria of fitting. The important structural parameters such as lattice parameters and cell volume values are summarized in Table 1. The fitting results are proved to be reliable with P4bm space group since the R_p , R_{wp} and χ^2 is relatively low. It is evident that the lattice parameters a , b , c and cell volume decrease with Ca content, also demonstrating the fact that Ca^{2+} ions are incorporated into the lattice (Fig. 2).

Figure 3 illustrates the SEM image of fresh surface of CSBN- x ceramics. The surface morphology of all samples presents a mixed characteristics of ordinary grains and rod-like grains. The sizes of two kinds grains show little difference among all samples. The average size of ordinary grains is about 2–3 μm while the mean size of rod-like grains significantly increases to 5–8 μm . As Ca content increased from 0.00 to 0.20, the porosity percentage of the samples varies

Fig. 1 a XRD pattern of CSBN-*x* ceramics, b The enlarged patterns for the (410) diffraction peak of all samples

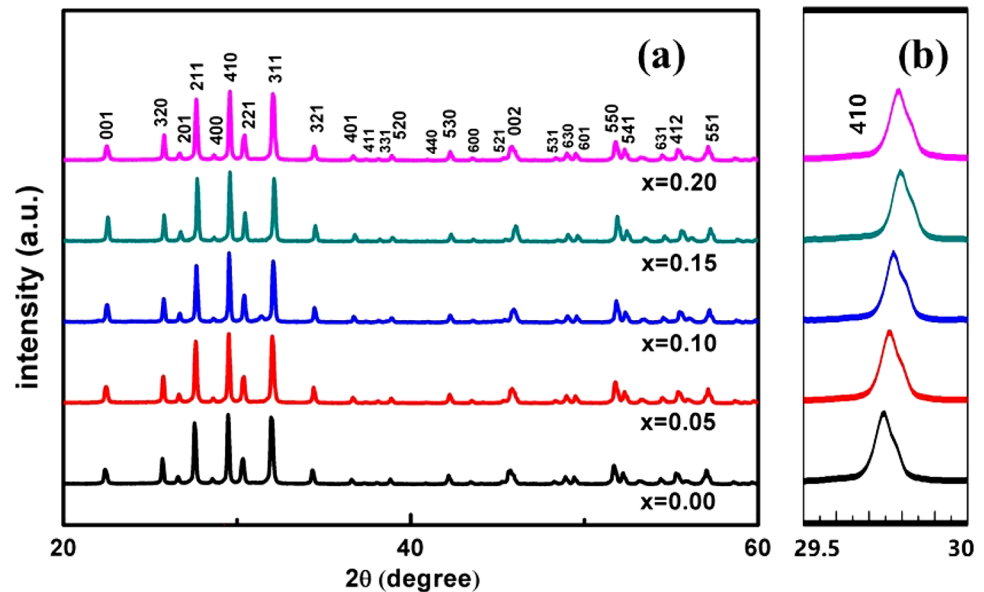


Table 1 Structural parameters determined from Rietveld refinement of CSBN-*x* ceramics

Ca content	Space group	Cell parameters				$R_p(\%)$	$R_{wp}(\%)$	χ^2
		$a = b(\text{Å})$	$c(\text{Å})$	$V_{\text{cell}} (\text{Å}^3)$	$\alpha = \beta = \gamma (^\circ)$			
0.00	P4bm	12.49510	3.96743	619.4250	90°	1.09	1.85	1.92
0.05	P4bm	12.48228	3.96011	617.0160	90°	1.14	1.87	1.98
0.10	P4bm	12.47483	3.95424	615.3613	90°	1.14	1.90	1.99
0.15	P4bm	12.46925	3.95252	614.5514	90°	1.09	1.84	1.91
0.20	P4bm	12.45985	3.94370	612.2510	90°	1.12	1.89	1.99

slightly (4.37%, 3.82%, 4.02%, 3.63% and 3.77% for $x = 0.00, 0.05, 0.10, 0.15$ and 0.20 , respectively).

3.2 Dielectric properties

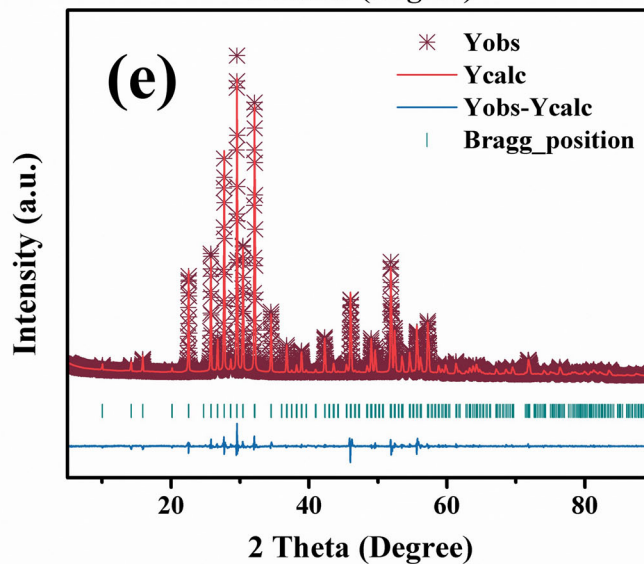
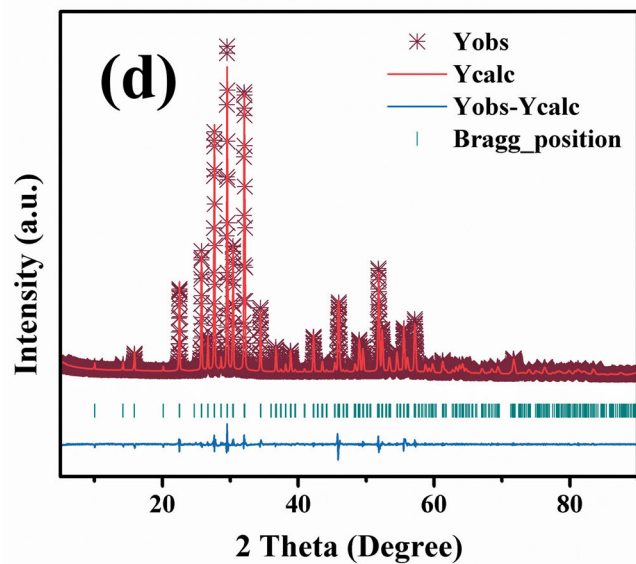
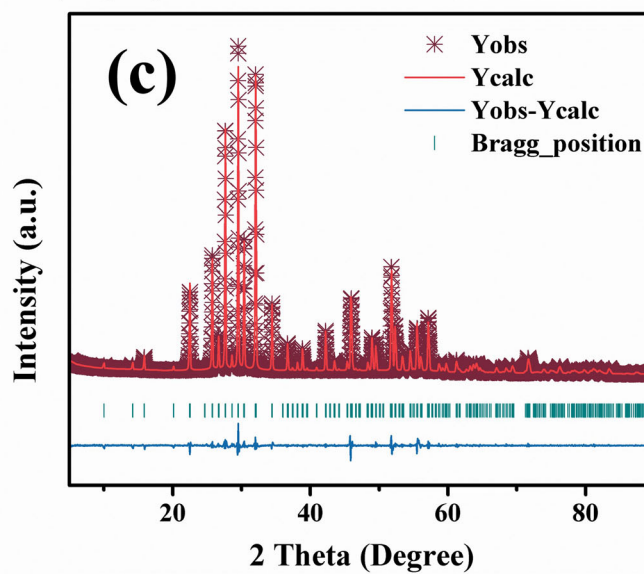
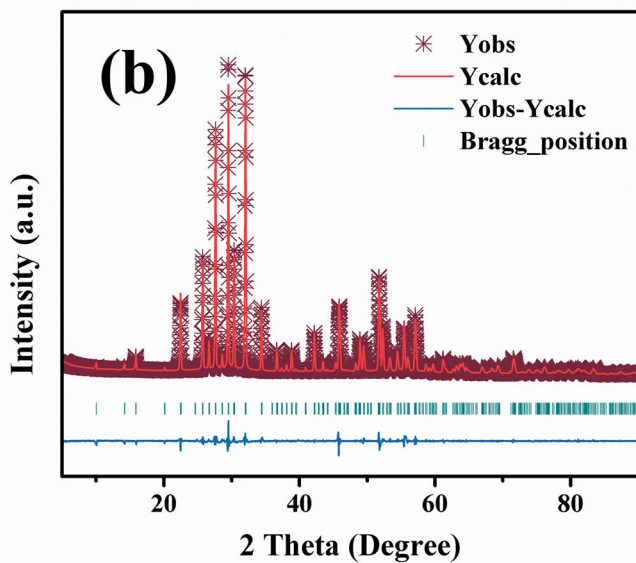
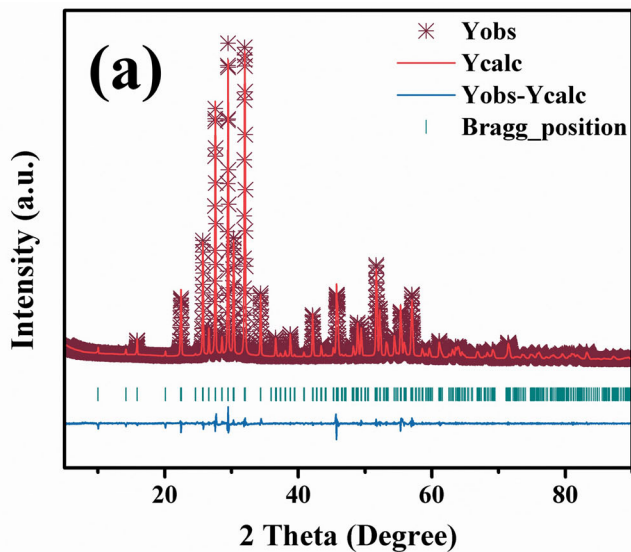
The temperature dependences of dielectric constant and loss for CSBN-*x* ceramics at the range of 100 Hz to 1 MHz are depicted in Fig. 4. The main dielectric phase transition parameters are listed in Table 1. The T_m representing the ferroelectric to paraelectric phase transition temperature is determined as the corresponding temperature of maximum dielectric constant (ϵ_m) at 1 kHz. As can be seen from Fig. 3, the T_m increases monotonically with Ca-substitution amount, which is 40.7°C for $x = 0.00$ and 90.0°C for $x = 0.20$. In CSBN crystal lattice, smaller Ca^{2+} (0.99 Å) and part of Sr^{2+} (1.13 Å) prefer to occupy the smaller A1-site (tetragonal interstices, with 12-fold coordination), while Ba^{2+} (1.35 Å) and residual Sr^{2+} jointly fill the larger A2-site (pentagonal interstices, with 15-fold coordination). When more and more

Ca^{2+} cations substitute Sr^{2+} cations in A1-site, the radius difference between A1-and A2-site cations will become larger, which is suggested to be the reason for elevating ferroelectric transition temperature in TTBS ceramics [29].

For ferroelectric relaxors, it is well known that the degree of the diffuseness can be described by a modified Curie–Weiss relationship: [32]

$$\frac{1}{\epsilon_r} - \frac{1}{\epsilon_m} = \frac{(T - T_m)^\gamma}{C}, 1 \leq \gamma \leq 2 \quad (1)$$

where ϵ_m is the maximum value of dielectric constant at the transition temperature, C represents the Curie constant and γ stands for the diffusivity parameter. Normally, $\gamma = 1$ is for normal ferroelectrics and $\gamma = 2$ is for ideal ferroelectric relaxors. The γ values, derived from fitting the plots of $\ln(1/\epsilon_r - 1/\epsilon_m)$ as a function of $\ln(T - T_m)$, are shown in Table 2. All the values are around 1.71–1.85 for both pure SBN and Ca-substituted SBN ceramics, indicating that all samples exhibit a typical diffuse transition and Ca-



◀ **Fig. 2** XRD Rietveld refinement for CSBN-x ceramics: **a** $x = 0.00$; **b** $x = 0.05$; **c** $x = 0.10$; **d** $x = 0.15$; **e** $x = 0.20$

substitution does not affect the relaxor behavior of SBN matrix.

In addition, the ferroelectric relaxor feature can also be depicted by the parameters of ΔT_{relax} . The specific symbols of the relaxation degree are defined as [33]:

$$\Delta T_{relax} = T_m(1\text{MHz}) - T_m(100\text{Hz}) \quad (2)$$

The values of ΔT_{relax} are calculated from experimental results and listed in Table 1 as well. With increasing Ca content, the value of ΔT_{relax} varies slightly, which is consistent with the diffusivity parameters. By using first-principle density functional calculations, G. H. Olsen et al. [34] found that the relaxor behavior in Sr-rich SBN originated from Sr displacement inside pentagonal channels (A2-sites) in the TTBS. Since Ca^{2+} is inclined to incorporate into A1-site, the amount of Sr^{2+} occupying A2-site in Sr-rich compositions remains constant after Ca-substitution, thus scarcely influencing the relaxation property of the samples.

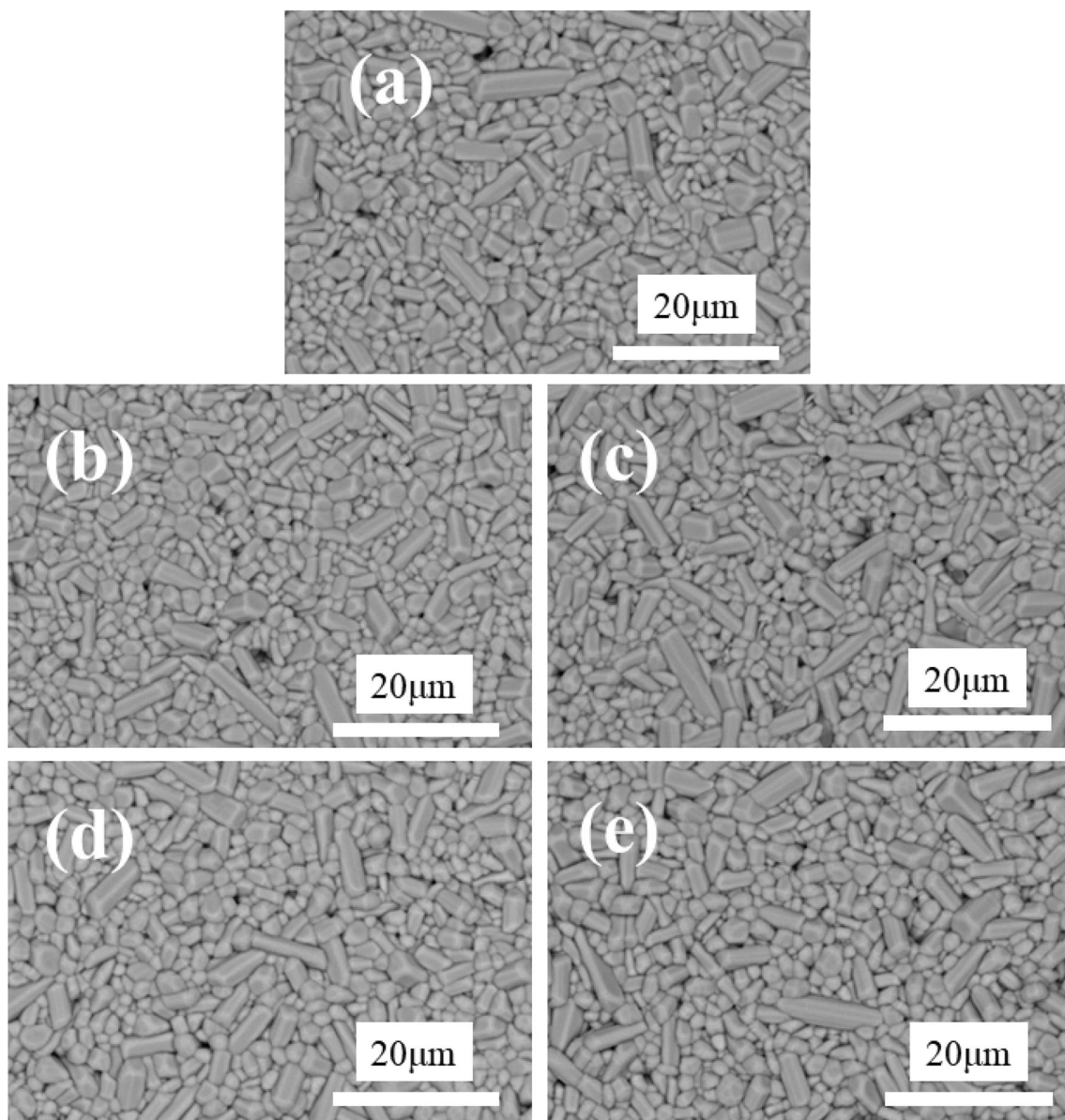


Fig. 3 SEM image of fresh surface of CSBN-x ceramics: **a** $x = 0.00$; **b** $x = 0.05$; **c** $x = 0.10$; **d** $x = 0.15$; **e** $x = 0.20$

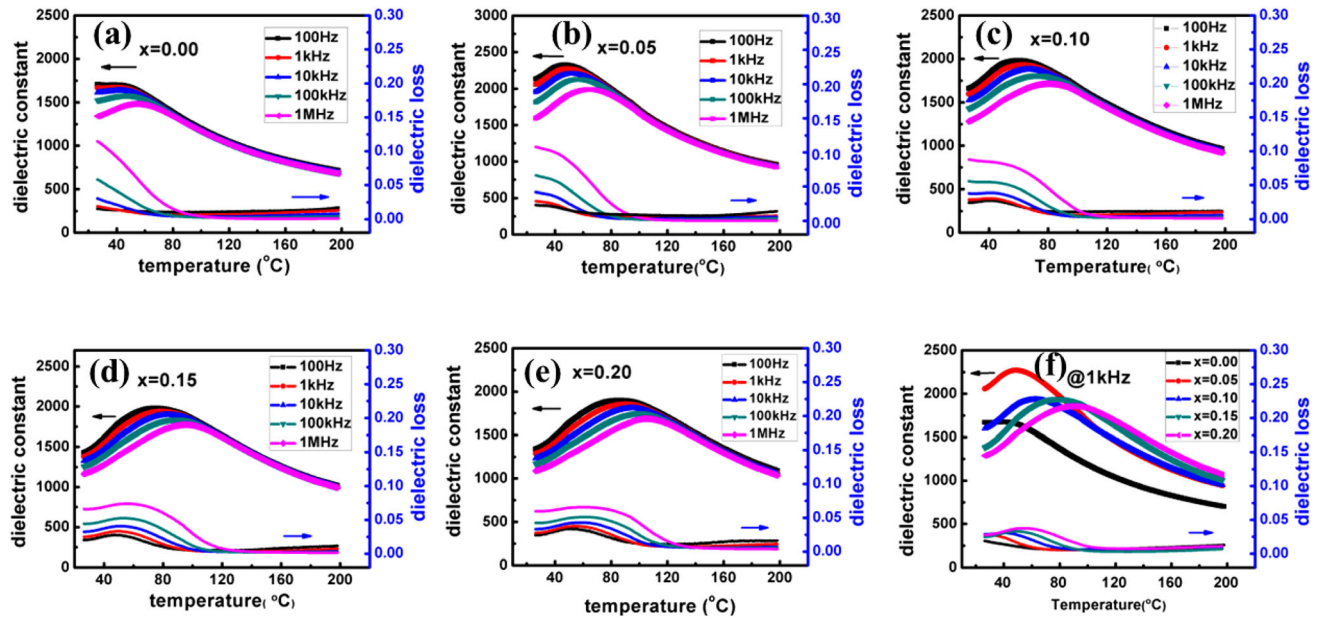


Fig. 4 The temperature dependences of dielectric constant and loss for CSBN-*x* ceramics at the range of 100 Hz to 1 MHz: **a** *x* = 0.00; **b** *x* = 0.05; **c** *x* = 0.10; **d** *x* = 0.15; **e** *x* = 0.20; **f** dielectric properties of CSBN-*x* ceramics with different *x* at 1 kHz

Table 2 Dielectric parameters for CSBN-*x* ceramics of different compositions

Parameters	Samples				
	<i>x</i> = 0.00	<i>x</i> = 0.05	<i>x</i> = 0.10	<i>x</i> = 0.15	<i>x</i> = 0.20
ϵ_m (1 kHz)	1672	2270	1930	1940	1855
ϵ_{RT} (1 kHz)	1668	2055	1596	1380	1288
T_m (1 kHz)/°C	40.7	48.8	63.2	79.0	90.0
T_m (100 Hz)/°C	38.6	47.2	60.6	74.1	87.3
T_m (1 MHz)/°C	53.9	64.7	80.5	95.0	105.0
γ (1 kHz)	1.78	1.72	1.71	1.85	1.76
ΔT_{relax} /°C	15.3	17.5	19.9	20.9	17.7

3.3 Ferroelectric and energy storage properties

Figure 4a shows the polarization versus applied electrical field (*P*-*E*) hysteresis loops of CSBN-*x* measured under 200 kV/cm at 10 Hz and room temperature and Fig. 4b demonstrates the variations of P_r , P_{max} , $P_{max}-P_r$, estimated from the loops. It can be seen that all samples present slim hysteresis loops. Compared with pure SBN sample, the introduction of Ca has greatly elevated the maximum polarization P_{max} from 13.2 μC/cm² for *x* = 0 to 17.9 μC/cm² for *x* = 0.15. Meanwhile, the remnant polarization P_r and coercive electric field E_c also increase monotonically in different degrees with increasing Ca content, indicating that the ferroelectricity is significantly enhanced by Ca addition. The value of $P_{max}-P_r$ shows

a tendency of increasing first and then decreasing and achieves the maximum at *x* = 0.05. It has been reported that the ferroelectricity in SBN system is determined by the atomic displacement (Δz) of the Nb⁵⁺ which is linearly proportional to the ferroelectric polarization [35]. Smaller Ca²⁺ substituting Sr²⁺ in A1-site could cause the twisting of the octahedral framework and changes in the O-Nb-O bonds, which probably gives rise to larger Δz and thus an enhancement in spontaneous polarization. The important ferroelectric polarization features extracted from *P*-*E* loops are summarized in Table 3 (Fig. 5).

The energy storage performance can be evaluated by following equations:

Table 3 Polarization features and energy storage properties of CSBN-*x* ceramics

Parameters	Samples				
	<i>x</i> = 0.00	<i>x</i> = 0.05	<i>x</i> = 0.10	<i>x</i> = 0.15	<i>x</i> = 0.20
P_{max} ($\mu\text{C}/\text{cm}^2$)	13.20	17.20	17.00	17.90	17.30
P_r ($\mu\text{C}/\text{cm}^2$)	0.69	1.03	1.59	2.85	3.14
$P_{max}-P_r$ ($\mu\text{C}/\text{cm}^2$)	12.51	16.17	15.41	15.05	14.16
W_{total} (J/cm^3)/ $^\circ\text{C}$	1.09	1.38	1.39	1.52	1.52
W_{rec} (J/cm^3)/ $^\circ\text{C}$	0.97	1.21	1.16	1.15	1.10
W_{loss} (J/cm^3)	0.12	0.17	0.23	0.37	0.42
η (%)	88.99	87.68	83.45	75.66	72.37

$$W_{total} = \int_0^{P_{max}} E dp \quad (3)$$

$$W_{rec} = \int_{P_r}^{P_{max}} E dp \quad (4)$$

$$W_{loss} = W_{total} - W_{rec} \quad (5)$$

$$\eta = \frac{W_{rec}}{W_{total}} \times 100\% \quad (6)$$

where W_{total} , W_{rec} and η are the total energy density, the recoverable energy storage density and the energy storage efficiency, respectively. In ferroelectric ceramic capacitors, due to noncoincidence of charging and discharging paths in hysteresis P - E loops, W_{total} representing the total charged energy cannot be released completely, while W_{rec} is the energy density that could be totally discharged and utilized. The W_{loss} equals to the difference between W_{total} and W_{rec} , which is wasted during the process and will generate heat within capacitors degrading the properties of capacitors. Energy storage efficiency η is the ratio of the discharged energy density (W_{rec}) to the charged energy density (W_{total}). Therefore, W_{rec} and η are important metrics to evaluate dielectrics' performance in energy storage application. The energy storage behaviors of CSBN-*x* ceramics are studied via P - E loops as shown in Fig. 6. The important energy storage properties are also listed in Table 3. Both W_{total} and W_{rec} increase after Ca-substitution. Particularly, W_{total} achieves the maximum values ($\sim 1.52 \text{ J}/\text{cm}^3$) in CSBN-15 composition, where W_{rec} is $1.15 \text{ J}/\text{cm}^3$ at ambient temperature. W_{rec} achieves the maximum values ($\sim 1.21 \text{ J}/\text{cm}^3$) at $x = 0.05$ and decreases slightly when further increasing the value of x , of which the trend is fully in line with that of $P_{max}-P_r$. Due to the elevation of P_r by introduction of Ca, the η shows a downward trend with increasing Ca content. The maximum $\eta = 88.99\%$ is obtained in

CSBN-0 samples, while the η drops to 72.37% at $x = 0.20$. In CSBN-5 samples, the energy storage efficiency η reaches as high as 87.68%, nearly equivalent to the value of pure SBN. In the whole, CSBN-5 composition presents the optimal overall energy storage properties with high W_{rec} ($1.21 \text{ J}/\text{cm}^3$) and η (87.68%) at room temperature. Figure 6b benchmarks the energy storage performance of the filled and unfilled TTBS ceramics systems in the recent literatures [15, 23–25, 36–46]. In comparison with the filled and unfilled TTBS ceramics systems, it is evident that the CSBN-5 ceramics simultaneously achieve high W_{rec} and high η , making it very attractive for energy storage application.

The good thermal stability is also an important parameter for practical energy storage application, for which guarantee the reliable operation of energy storage devices over a wide temperature range. To evaluate the thermal stability performance of CSBN-5 sample, its hysteresis loops are measured in the temperature range of $25 \text{ }^\circ\text{C}$ – $20 \text{ }^\circ\text{C}$ at $200 \text{ kV}/\text{cm}$, as shown in Fig. 7a. The slim hysteresis loops are maintained throughout the testing temperature range, with a slight decrease in P_{max} and P_r . Specifically, the P_{max} of CSBN-5 is $17.20 \mu\text{C}/\text{cm}^2$ at $25 \text{ }^\circ\text{C}$ while it still maintains 89.5% of the initial value at $120 \text{ }^\circ\text{C}$ ($15.4 \mu\text{C}/\text{cm}^2$). In the meantime, the P_r has reduced from $1.03 \mu\text{C}/\text{cm}^2$ around ambient temperature to $0.70 \mu\text{C}/\text{cm}^2$ at $120 \text{ }^\circ\text{C}$. The difference between P_{max} and P_r ($P_{max}-P_r$) at each temperature declines to a small extent over this range, implying tiny reduction in recoverable energy storage density. The W_{rec} , W_{loss} and η of CSBN-5 composition at each temperature calculated from the P - E loops are also shown in Fig. 7b. The flat curve reflects the stable W_{rec} value over the test temperature with a maximum of $1.21 \text{ J}/\text{cm}^3$ and a minimum of $1.19 \text{ J}/\text{cm}^3$. Of particular interest is that the η slightly

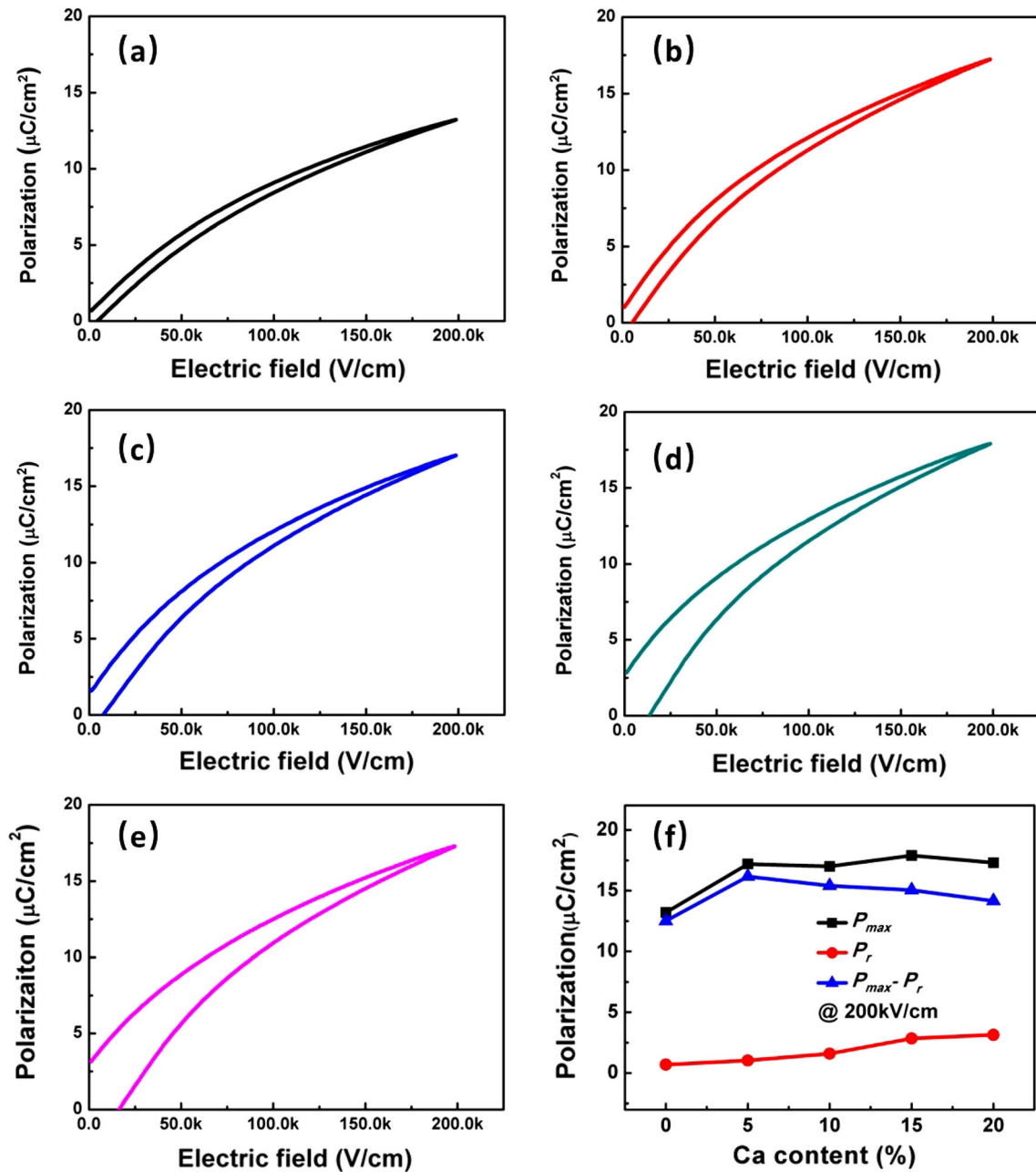


Fig. 5 The polarization versus applied electrical field (P - E) hysteresis loops of CSBN- x measured under 200 kV/cm at 1 Hz and room temperature: **a** $x = 0.00$; **b** $x = 0.05$; **c** $x = 0.10$;

increases towards elevated temperature due to the declined P_r . The room temperature η is 87.68% while it reaches as high as 90.32% at 120 °C. Overall, the variations of W_{rec} and η are respectively on the order of < 2% and 3% within the temperature range, demonstrating quite good thermal stability performance of this composition.

d $x = 0.15$; **e** $x = 0.20$; **f** Variations of P_r , P_{max} , $P_{max} - P_r$ estimated from P - E loops for CSBN- x ceramics

4 Conclusions

Tetragonal tungsten bronze structure $\text{Ca}_x\text{Sr}_{0.75-x}\text{Ba}_{0.25}\text{Nb}_2\text{O}_6$ ($x = 0.00, 0.05, 0.10, 0.15, 0.20$) lead-free ferroelectric relaxor ceramics have been synthesized via conventional solid-state reaction route. Enhanced dielectric and ferroelectric properties with increased ferroelectric transition temperature T_m and maximum

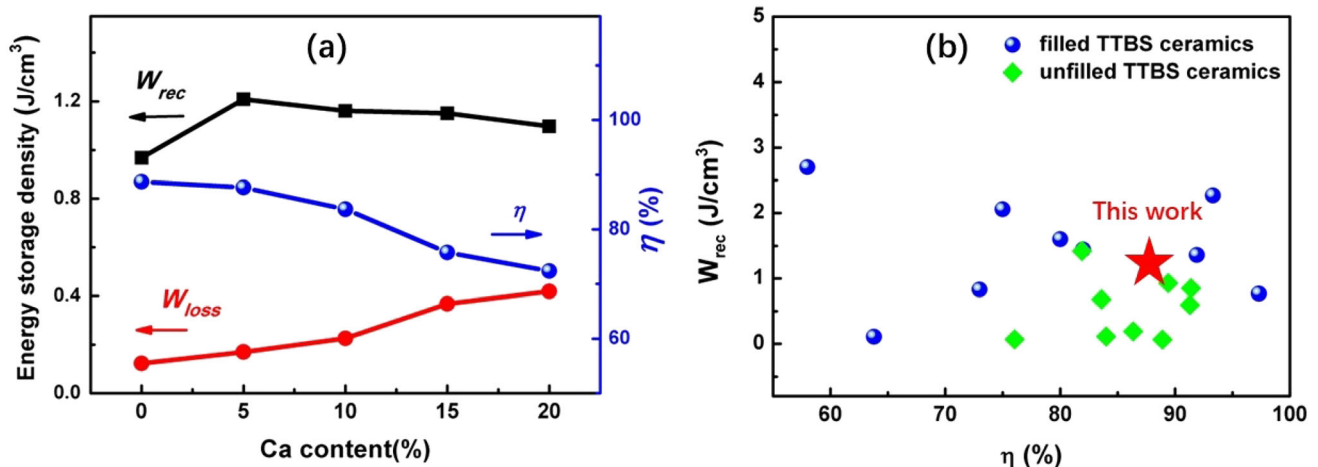


Fig. 6 a Energy storage performance of CSBN- x ceramics under 200 kV/cm; b Comparison of W_{rec} and η among CSBN-5 and other TTBS ceramics [15, 23–25, 36–46]

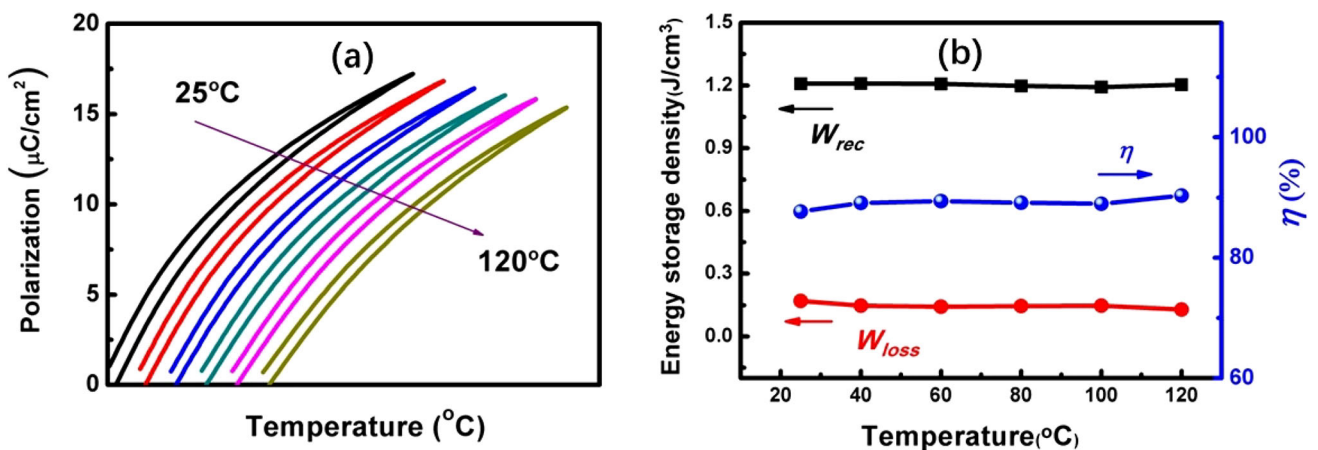


Fig. 7 a The hysteresis loops of CSBN-5 ceramics in the range of 25 $^{\circ}C$ –120 $^{\circ}C$ at 200 kV/cm; b the W_{rec} , W_{loss} and η values of CSBN-5 ceramics in the range of 25 $^{\circ}C$ –120 $^{\circ}C$ at 200 kV/cm

polarization P_{max} are achieved in CSBN- x ceramics due to the enhancement of structure distortion by smaller Ca^{2+} substituting Sr^{2+} . The optimal energy storage properties, *i.e.* high recoverable energy storage density W_{rec} (1.21 J/cm^3) and energy storage efficiency η (87.68%), ultrahigh temperature stability (the fluctuations on W_{rec} and η are within 2% and 3% over the range of 25 $^{\circ}C$ –120 $^{\circ}C$, respectively) are obtained in $Ca_{0.05}Sr_{0.70}Ba_{0.25}Nb_2O_6$ composition, unveiling the potential of CSBN-5 lead-free ferroelectric relaxor ceramics for energy storage application.

Author contributions

SG: implemented the research scheme and wrote the manuscript. CY: helped to make material preparation. FC: provided support for the electrical properties measurements. ZL: reviewed and edited the article. GW: reviewed and edited the article.

Funding

This work was supported by the Key Deployment Projects of Chinese Academy of Sciences (Grant No. ZDRW-CN-2021-3-1-18) and the National Natural Science Foundation of China (NSFC) (Grant No. 61475176).

Data availability

The data used to support the findings of this study are included within the article.

Declarations

Conflict of interest The authors declare that they have no known competing financial interests or personal relationships that could have appeared to influence the work reported in this paper.

Ethical approval This article does not contain any studies involving humans and animals performed by any of the authors.

References

- B.J. Chu, X. Zhou, K.L. Ren, B. Neese, M.R. Lin, Q. Wang, F. Bauer, Q.M. Zhang, *Science* **313**, 334 (2006)
- L.T. Yang, X. Kong, F. Li, H. Hao, Z.X. Cheng, H.X. Liu, J.F. Li, S.J. Zhang, *Prog. Mater. Sci.* **102**, 72 (2019)
- Z.H. Yao, Z. Song, H. Hao, Z.Y. Yu, M.H. Cao, S.J. Zhang, M.T. Lanagan, H.X. Liu, *Adv. Mater.* **29**, 1601727 (2017)
- Z. Liu, T. Lu, J.M. Ye, G.S. Wang, X.L. Dong, R. Withers, Y. Liu, *Adv. Mater. Technol.* **3**, 1800111 (2018)
- M.X. Zhou, R.H. Liang, Z.Y. Zhou, X.L. Dong, *J. Mater. Chem. C* **6**, 8528 (2018)
- T. Wang, L. Jin, C. Li, Q.Y. Hu, X.Y. Wei, *J. Am. Ceram. Soc.* **98**, 559 (2015)
- P.Y. Zhao, H.X. Wang, L.W. Wu, L.L. Chen, Z.M. Cai, L.T. Li, X.H. Wang, *Adv. Energy Mater.* **9**, 1803048 (2019)
- Q.Y. Hu, Y. Tian, Q.S. Zhu, J.H. Bian, L. Jin, H.L. Du, D.O. Alikin, V.Y. Shur, Y.J. Feng, Z. Xu, X.Y. Wei, *Nano Energy* **67**, 104264 (2020)
- W. Wang, L.Y. Zhang, R.Y. Jing, Q.Y. Hu, D.O. Alikin, V.Y. Shur, X.Y. Wei, G. Liu, Y. Yan, L. Jin, *Chem. Eng. J.* **434**, 134678 (2022)
- A.W. Xie, R.Z. Zuo, Z.L. Qiao, Z.Q. Fu, T.F. Hu, L.F. Fei, *Adv. Energy Mater.* **11**, 2101378 (2021)
- D. Hu, Z.B. Pan, X. Zhang, H.R. Ye, Z.Y. He, M.K. Wang, S. Xing, J.W. Zhai, Q. Fu, J.J. Liu, *J. Mater. Chem. C* **8**, 591 (2020)
- A. Zhang, H.B. Yang, Y. Lin, Q.B. Yuan, H.L. Du, *Energy Stor. Mater.* **45**, 861 (2022)
- Y. Slimani, A. Selmi, E. Hannachi, M.A. Almessiere, G. Alfalah, L.F. Alousi, G. Yasin, M. Iqbal, *J. Phys. and Chem. Solids* **156**, 110183 (2021)
- M.P. Trubelja, E. Ryba, D.K. Smith, *J. Mater. Sci.* **31**, 1435 (1996)
- L. Cao, Y. Yuan, Z.Y. Yang, E.Z. Li, S.R. Zhang, *Ceram. Int.* **46**, 6108 (2020)
- J. Gardner, F.D. Morrison, *Dalton Trans.* **43**(30), 11687 (2014)
- A.M. Glass, *Appl. Phys. Lett.* **13**(4), 147 (1968)
- A.M. Glass, *J. Appl. Phys.* **40**(12), 4699 (1969)
- P. Molina, M.D. Ramirez, L.E. Bausa, *Adv. Funct. Mater.* **18**(5), 709 (2008)
- J. Zhang, G.S. Wang, F. Gao, C.L. Mao, X.L. Dong, *Ceram. Int.* **39**(2), 1971 (2013)
- S. Podlozhenov, H.A. Graetsch, J. Schneider, M. Ulex, M. Wohlecke, K. Betzler, *Acta Cryst. B* **62**, 960 (2006)
- T.S. Chernaya, B.A. Maksimov, T.R. Volk, L.I. Ivleva, V.I. Simonov, *Phys. Solid State* **42**(9), 1716 (2000)
- H. Bai, J. Li, Y. Wu, Y. Hong, K.Z. Shi, Z.X. Zhou, *Ceram. Int.* **45**, 11109 (2019)
- H. Tang, X.G. Tang, M.D. Li, Q.X. Liu, Y.P. Jiang, *J. Alloys Compd.* **791**, 1038 (2019)
- Y. Rao, H.X. Liu, H. Hao, Z.H. Yao, X.X. Zhou, M.H. Cao, Z.Y. Yu, *Ceram. Int.* **44**, 11022 (2018)
- S. Dursun, E. Mensur-Alkoy, S. Alkoy, *J. Eur. Ceram. Soc.* **36**, 2479 (2016)
- Y.J. Qi, C.J. Lu, J. Zhu, J. Zhu, X.B. Chen, X.G. Xu, *Appl. Phys. Lett.* **87**, 167 (2005)
- J. Zhang, X.L. Dong, F. Cao, S.B. Guo, G.S. Wang, *Appl. Phys. Lett.* **102**, 3495 (2013)
- H. Chen, S.B. Guo, X.L. Dong, F. Cao, C.L. Mao, G.S. Wang, *J. Alloys Compd.* **695**, 2723 (2017)
- R.J. Xie, Y. Akimune, K. Matsuo, T. Sugiyama, N. Hirotsuki, T. Sekiya, *Appl. Phys. Lett.* **80**, 835 (2002)
- Y.B. Yao, C.L. Mak, *J. Alloys Compd.* **544**, 87 (2012)
- K. Uchino, S. Nomura, *Ferroelectr. Lett.* **44**, 55 (1982)
- W. Chen, X. Yao, X.Y. Wei, *Appl. Phys. Lett.* **90**, 2289 (2007)
- G.H. Olsen, U. Aschauer, N.A. Spaldin, S.M. Selbach, T. Grande, *Phys. Rev. B* **93**, 180101 (2016)
- S.C. Abrahams, S.K. Kurtz, P.B. Jamieson, *Phys. Rev.* **172**, 551 (1968)
- R. Li, Y.P. Pu, Q.W. Zhang, W. Wang, J.W. Li, X.Y. Du, M. Chen, X. Zhang, Z.X. Sun, *J. Eur. Ceram. Soc.* **40**, 4509 (2020)
- S.D. Xu, S.J. Shen, C.W. Huang, Y. He, X.L. Chao, D. Wu, P.F. Liang, Z.P. Yang, J.B. Lu, L.L. Wei, *ACS Appl. Interfaces Mater.* (2023). <https://doi.org/10.1021/acsami.2c18827>
- B. Yang, S.L. Hao, P. Yang, L.L. Wei, Z.P. Yang, *Ceram. Int.* **44**, 8832 (2018)
- S.D. Xu, S.J. Shen, R. Hao, Z.H. Peng, F.D. Zhang, D. Wu, P.F. Liang, X.L. Chao, L.L. Wei, Z.P. Yang, *Chem. Eng. J.* **433**, 133812 (2022)

40. L. Cao, Y. Yuan, B. Tang, E.Z. Li, S.R. Zhang, J. Eur. Ceram. Soc. **40**, 2366 (2020)
41. W.B. Feng, Y.F. Xu, X.G. Li, Y.Y. Wu, J.J. Yang, J. Mater. Sci.: Mater. Electron **34**, 117 (2023)
42. X. Zheng, Z.H. Jin, Y.J. Dan, C.Z. Hu, L.J. Liu, L. Fang, J. Mater. Sci.: Mater. Electron **34**, 148 (2023)
43. S.D. Xu, R. Hao, Z. Yan, S.T. Hou, Z.H. Peng, D. Wu, P.F. Liang, X.L. Chao, L.L. Wei, Z.P. Yang, J. Eur. Ceram. Soc. **42**, 2781 (2022)
44. S.T. Hou, S.D. Xu, L.J. Yang, X. Liu, L.L. Wei, X.L. Chao, D. Wu, P.F. Liang, Z.P. Yang, Ceram. Int. (2022). <https://doi.org/10.1016/j.ceramint.2022.06.148>
45. Y.Y. Zhao, J.P. Wang, L.X. Zhang, X.J. Shi, S.J. Liu, D.W. Zhang, Ceram. Int. **42**, 16697 (2016)
46. G.H. Chen, J. Zheng, Z.C. Li, J.W. Xu, Q.N. Li, C.R. Zhou, C.L. Yuan, Q. Feng, J. Mater. Sci.: Mater. Electron **27**, 2645 (2016)

Publisher's Note Springer Nature remains neutral with regard to jurisdictional claims in published maps and institutional affiliations.

Springer Nature or its licensor (e.g. a society or other partner) holds exclusive rights to this article under a publishing agreement with the author(s) or other rightsholder(s); author self-archiving of the accepted manuscript version of this article is solely governed by the terms of such publishing agreement and applicable law.